Environmental enrichment does not seem generally to increase variability, although some controversy exists with regard to parameters such as body weight (*17*, *25*, *26*). Most studies, however, have followed smaller cohorts of animals over shorter periods of time than in our study. Whether long-term enrichment in large groups and seminaturalistic conditions have a general variance-increasing effect across a wide range of parameters remains to be determined.

Three months of living in a complex environment led to a massive magnification of individual differences in explorative behavior among genetically identical individuals over time, and these differences were related to adult hippocampal neurogenesis. The rich environment lost its "sameness" over time and gave way to the emergence of a personalized "life space" (*27*) and a "mouse individuality," similar to what has been observed in humans for personality traits (*28*). Hence, the magnitude of individual differences observed in replications of this experiment is likely to vary across studies: As the members of each new cohort individualize, their "society" will also be shaped in a slightly different, individual way. The present paradigm serves as an animal model for addressing the "mystery and controversy" (*2*) of the nonshared environment, or the ways in which living our lives makes us who we are (*29*).

### References and Notes


1. P. C. M. Molenaar, D. I. Boomsma, C. V. Dolan, in *Problems and Methods in Longitudinal Research: Stability and Change*, D. Magnusson, G. Bergman, B. Rudinger, B. Törstad, Eds. (Cambridge Univ. Press, Cambridge, 1991), pp. 250–273.
2. E. Turkheimer, *Psychol. Bull.* **137**, 825 (2011).
3. M. R. Rosenzweig, E. L. Bennett, *Behav. Brain Res.* **78**, 57 (1996).
4. H. van Praag, G. Kempermann, F. H. Gage, *Nat. Rev. Neurosci.* **1**, 191 (2000).
5. A. E. Whimbey, V. H. Denenberg, *Behaviour* **29**, 296 (1967).
6. L. Lewejohann, B. Zipser, N. Sachser, *Dev. Psychobiol.* **53**, 624 (2011).
7. G. Kempermann, *Trends Neurosci.* **31**, 163 (2008).
8. L. Lewejohann *et al.*, *Behav. Res. Methods* **41**, 850 (2009).
9. B. Steiner *et al.*, *Glia* **46**, 41 (2004).
10. A. Garthe, J. Behr, G. Kempermann, *PLoS ONE* **4**, e5464 (2009).
11. G. Kempermann, *Nat. Rev. Neurosci.* **13**, 727 (2012).
12. G. Kempermann *et al.*, *Front Neurosci* **4**, 189 (2010).
13. K. Fabel *et al.*, *Front. Neurosci.* **3**, 50 (2009).
14. I. Amrein, H. P. Lipp, *Biol. Lett.* **5**, 141 (2009).
15. G. Kempermann, *J. Neurosci.* **22**, 635 (2002).
16. J. C. Crabbe, D. Wahlsten, B. C. Dudek, *Science* **284**, 1670 (1999).
17. L. Lewejohann *et al.*, *Genes Brain Behav.* **5**, 64 (2006).
18. D. W. Bailey, *Immunol. Today* **3**, 210 (1982).
19. R. Lathe, *Genes Brain Behav.* **3**, 317 (2004).
20. C. Julier *et al.*, *Proc. Natl. Acad. Sci. U.S.A.* **87**, 4585 (1990).
21. R. P. Talens *et al.*, *Aging Cell* **11**, 694 (2012).
22. P. B. Baltes, J. R. Nesselroade, S. W. Cornelius, *Multivariate Behav. Res.* **13**, 127 (1978).
23. M. E. Raijmakers, P. C. Molenaar, *Dev. Sci.* **7**, 149 (2004).
24. K. Friston, M. Breakspear, G. Deco, *Front. Comput. Neurosci.* **6**, 44 (2012).
25. H. A. Van de Weerd *et al.*, *J. Appl. Anim. Welf. Sci.* **5**, 87 (2002).
26. D. P. Wolfer *et al.*, *Nature* **432**, 821 (2004).
27. K. Lewin, *Dynamic Theory of Personality* (McGraw-Hill, New York, 1935).
28. K. L. Jang, R. R. McCrae, A. Angleitner, R. Riemann, W. J. Livesley, *J. Pers. Soc. Psychol.* **74**, 1556 (1998).
29. P. C. Molenaar, D. I. Boomsma, C. V. Dolan, *Behav. Genet.* **23**, 519 (1993).


**Acknowledgments:** This study was financed from basic institutional funds. J.F. and I.K. were fellows of the International Max Planck Research School on the Life Course (LIFE), Berlin. M.K. has been supported by the International Research Training Group on Semantic Integration of Geospatial Information, funded by the German Research Foundation (DFG). The authors thank S. Vogler for drawing the cage in Fig. 1A and D. Lasse for technical support. G.K. and U.L. would also like to thank J. Nesselroade for inspiring discussions that helped shape the ideas presented in this report.

### Supplementary Materials

www.sciencemag.org/cgi/content/full/340/6133/756/DC1
Materials and Methods
Figs. S1 and S2
References (*30*–*35*)
Movies S1 and S2

17 January 2013; accepted 22 March 2013
10.1126/science.1235294

# Compartmentalization of GABAergic Inhibition by Dendritic Spines

**Chiayu Q. Chiu,[1,2]* Gyorgy Lur,[1,2]* Thomas M. Morse,[1] Nicholas T. Carnevale,[1] Graham C. R. Ellis-Davies,[3] Michael J. Higley[1,2]†**

**γ-aminobutyric acid–mediated (GABAergic) inhibition plays a critical role in shaping neuronal activity in the neocortex. Numerous experimental investigations have examined perisomatic inhibitory synapses, which control action potential output from pyramidal neurons. However, most inhibitory synapses in the neocortex are formed onto pyramidal cell dendrites, where theoretical studies suggest they may focally regulate cellular activity. The precision of GABAergic control over dendritic electrical and biochemical signaling is unknown. By using cell type-specific optical stimulation in combination with two-photon calcium ($Ca^{2+}$) imaging, we show that somatostatin-expressing interneurons exert compartmentalized control over postsynaptic $Ca^{2+}$ signals within individual dendritic spines. This highly focal inhibitory action is mediated by a subset of GABAergic synapses that directly target spine heads. GABAergic inhibition thus participates in localized control of dendritic electrical and biochemical signaling.**

A challenge to elucidating the function of synaptic inhibition is the diversity of γ-aminobutyric acid–releasing (GABAergic) interneurons found in cortical circuits (*1*–*3*). Several interneuron classes, including those that express somatostatin (SOM-INs), target the dendrites of excitatory, glutamatergic pyramidal cells (*3*–*5*). SOM-INs regulate the initiation of action potential bursts generated via active currents in postsynaptic dendrites (*6*–*8*). We hypothesized that these inputs might also exert focal influence over dendritic signaling. Here, we used electrophysiological, optical, and computational approaches to investigate the localized actions of GABAergic inhibition in pyramidal cell dendrites.

To activate dendritic GABAergic synapses, we used a somatostatin-Cre mouse line (*9*) (Fig. 1A and fig. S1, A and B) to conditionally express channelrhodopsin-2 (ChR2) (*10*) in SOM-INs of the prefrontal cortex (fig. S1, C and D). In acute brain slices prepared 2 to 3 weeks after viral injection, pulses of light (5 ms, 473 nm) delivered through the microscope objective evoked action potentials (APs) in fluorescently identified SOM-INs (fig. S2, A to C). Whole-cell recordings in layer 2/3 pyramidal neurons revealed corresponding inhibitory postsynaptic potentials (IPSPs) (Fig. 1, B and C, and fig. S2, D to F). For subsequent experiments, type A GABA receptor ($GABA_AR$)–mediated IPSPs were isolated by including the selective type B GABA receptor ($GABA_BR$) antagonist CGP-55845 in the perfusate (Fig. 1C). IPSPs exhibited a reversal potential of –69.9 ± 1.5 mV (mean ± SEM, $n = 5$) that did not differ significantly from the value recorded via gramicidin-based perforated patch (–72.4 ± 1.7, $n = 6$, $P = 0.3$, fig. S2, G and H).

To determine how inhibition influences dendritic activity in pyramidal neurons, we used two-photon laser scanning microscopy (2PLSM) to image calcium ($Ca^{2+}$) in apical dendritic spines and shafts. $Ca^{2+}$ transients ($\Delta Ca^{2+}$) were evoked by somatic APs (Fig. 1, D and E, and fig. S3, A and B) and were mediated by voltage-gated $Ca^{2+}$ channels (VGCCs) (fig. S3C). We compared AP-evoked $Ca^{2+}$ signals under control conditions ($\Delta Ca^{2+}_{ctl}$) and when preceded by an IPSP ($\Delta Ca^{2+}_{inh}$) (15-ms interval) evoked by a light pulse targeting the imaged region (Fig. 1E). In 57% (73/127) of randomly imaged spines, optical activation of SOM-INs produced a significant reduction (>15%, see methods and fig. S3, D to F) in the AP-evoked $\Delta Ca^{2+}$. At these locations, the average $Ca^{2+}$ inhibition ($\Delta Ca^{2+}_{inh}/\Delta Ca^{2+}_{ctl}$) was significantly greater for spines than for neighboring dendritic shafts (0.60 ± 0.02 versus 0.78 ± 0.03, $P < 0.001$; Fig. 1, F and G). The inhibition of $\Delta Ca^{2+}$ was abolished by application of the $GABA_A$ antagonist picrotoxin ($n = 8$, $P < 0.05$, Fig. 1H). Similar $Ca^{2+}$ inhibition was seen in basal dendrites (23/49 spines; 0.73 ± 0.02 versus 0.87 ± 0.02 for spines and shafts, respectively, $P < 0.01$; fig. S4).

[1]Department of Neurobiology, Yale School of Medicine, New Haven, CT 06510, USA. [2]Yale Program in Cellular Neuroscience, Neurodegeneration, and Repair, Yale School of Medicine, New Haven, CT 06510, USA. [3]Department of Neuroscience, Mount Sinai School of Medicine, New York, NY 10029, USA.

*These authors contributed equally to this work.
†Corresponding author. E-mail: m.higley@yale.edu

We frequently observed inhibited and uninhibited spines in close proximity, suggesting compartmentalized GABAergic control of $Ca^{2+}$ signaling. We therefore imaged $Ca^{2+}$ inhibition within a small dendritic region. Spines adjacent to an inhibited reference spine typically showed little modulation despite the presence of a somatic IPSP (Fig. 2, A and B, and fig. S5, A and B). We generated "maps" demonstrating heterogeneous inhibition over short distances (Fig. 2C). There was significantly greater inhibition for each reference spine than for its adjacent neighbor ($0.58 \pm 0.03$ versus $0.82 \pm 0.03$, $P < 0.001$, $n = 22$ maps), and inhibition between neighbors was not correlated (Pearson $r^2 = 0.12$, $P = 0.09$, Fig. 2H). Inhibition in individual spines was not correlated to the magnitude of $\Delta Ca^{2+}_{ctl}$ (fig. S5C) and was unchanged for experiments conducted at near-physiological temperature or with $GABA_BR$ function intact (fig. S5D).

We further characterized inhibitory compartmentalization by using photoactivation of the caged compound RuBi-GABA (*11*). Brief light pulses (2 ms, 473 nm) evoked IPSPs in pyramidal neurons bathed in RuBi-GABA (10.8 μM) with much smaller amplitudes but similar kinetics as those produced by stimulation of SOM-INs (fig. S6, A to C). By using GABA uncaging, we found that 51% (44/87) of randomly imaged apical spines showed significant inhibition of $\Delta Ca^{2+}$. Inhibition was stronger in spines than in dendritic shafts ($0.65 \pm 0.02$ versus $0.79 \pm 0.03$, $P < 0.0001$, $n = 59$; Fig. 2, G and fig. S6D) and was blocked by picrotoxin (fig. S6, E and F). Inhibitory compartmentalization was similar to that seen by using optical stimulation of SOM-INs (Fig. 2, D to F). $Ca^{2+}$ inhibition for the reference spine was significantly greater than for the adjacent neighbor ($0.64 \pm 0.05$ versus $0.90 \pm 0.06$, $P < 0.01$, $n = 15$ maps), and these values were uncorrelated (Pearson $r^2 = 0.11$, $P = 0.22$, Fig. 2I).

Increasing intracellular chloride caused IPSPs to be depolarizing from a membrane potential ($V_m$) of –60 mV and largely eliminated inhibition of $\Delta Ca^{2+}$ ($n = 24$, $P < 0.0001$ versus control, fig. S7, A and B), suggesting that local membrane hyperpolarization contributes to reduced $Ca^{2+}$ influx. VGCCs with more depolarized activation thresholds should therefore exhibit greater sensitivity to GABAergic inhibition. Indeed, blockade of high-threshold (L and N/P/Q types) but not lower-threshold (T and R types) channels significantly reduced the amount of $Ca^{2+}$ inhibition evoked by GABA uncaging (fig. S7C).

Many spines receive direct GABAergic input (*5*, *12*, *13*), and we wondered whether SOM-INs might contribute to this pool of synapses. We reconstructed apical dendrites of recorded neurons from ChR2 experiments and found 18.5% of spines ($n = 1185$ spines, 4 cells) expressed the inhibitory synaptic protein gephyrin, whereas 43.5% ($n = 3058$ spines, 9 cells) appeared to be contacted by a presynaptic bouton originating from a SOM-IN (fig. S8, A and B; see methods). For a subset of cells ($n = 3$), we recovered spines with corresponding $Ca^{2+}$ imaging. In all cases, $Ca^{2+}$ inhibition was only observed for spines with an apposed SOM-IN terminal (Fig. 3, A to C, and fig. S8, C to H).

We next confirmed the spatial precision of GABAergic inhibition by using diffraction-limited two-photon laser uncaging (2PLU) of 4-carboxymethoxy-5,7-dinitro-indolinyl (CDNI)–GABA (*14*) (methods). The $Ca^{2+}$ inhibition evoked by $2PLU_{GABA}$ was similar in magnitude to that produced by ChR2 activation, highly sensitive to the precise location of the uncaging spot around the spine perimeter, and isolated from neighboring spines (Fig. 3, D to G).

To see whether GABAergic synapses onto spines are necessary for compartmentalized inhibition, we simulated AP-evoked $Ca^{2+}$ influx into dendritic spines and shafts (Fig. 3H, fig. S9, and methods). GABAergic input to a single spine head inhibited $\Delta Ca^{2+}$ only in the targeted spine, whereas inhibition targeting the dendritic shaft had minimal effect on nearby spines (Fig. 3I). Moreover, $\Delta Ca^{2+}$ in the dendritic shaft was unaffected by GABAergic input to either the spine head or shaft (Fig. 3J). $Ca^{2+}$ inhibition was mediated by a compartmentalized reduction in input impedance, reducing AP amplitude in the targeted spine (fig. S9, A to D). The magnitude of inhibition was influenced by spine neck resistance, chloride reversal potential, and VGCC activation threshold but was independent of VGCC density (fig. S9, E to G). Inhibition (>15%) of dendritic $\Delta Ca^{2+}$ could only be obtained by increasing the dendritic GABAergic conductance 10-fold (fig. S9H). A current-based inhibitory synapse that generated a similar IPSP in the absence of a conductance change produced minimal $Ca^{2+}$ inhibition (fig. S9I).

Lastly, we asked whether localized inhibition occurred for synaptic $Ca^{2+}$ transients and excitatory postsynaptic potentials (EPSPs). We combined one-photon RuBi-GABA uncaging with

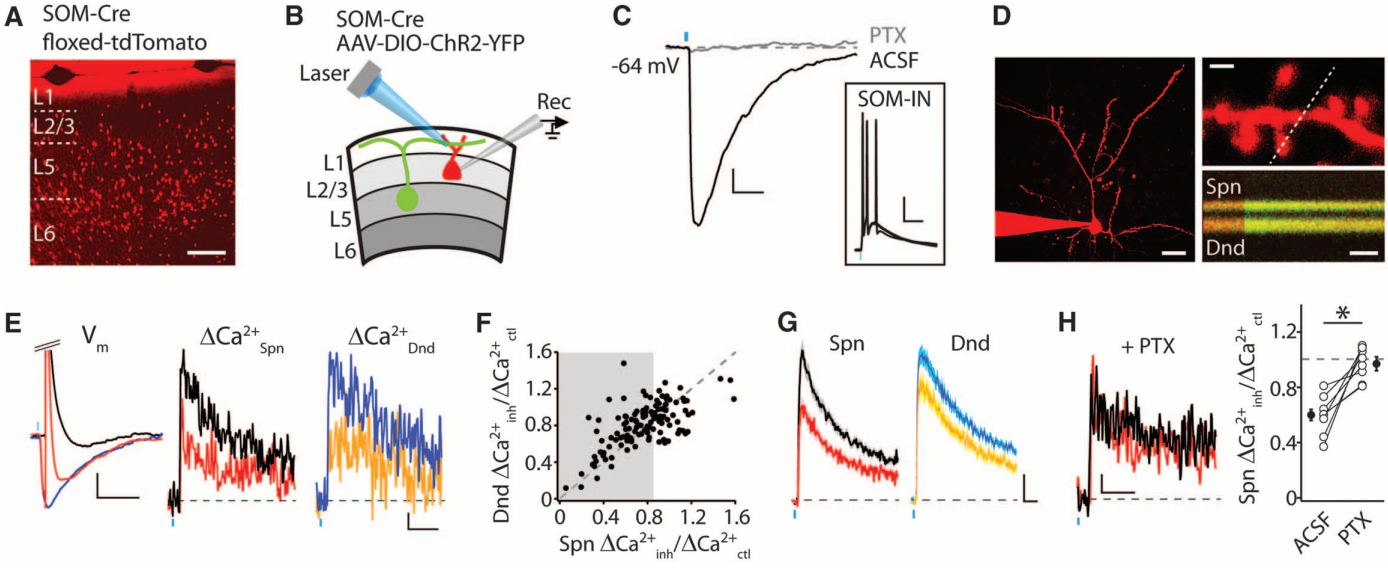


**Fig. 1. SOM-INs mediate inhibition of dendritic $Ca^{2+}$ signals.** (**A**) tdTomato expression in the prefrontal cortex of SOM-Cre;Ai9 mice. Scale bar indicates 200 μm. (**B**) Recording configuration. (**C**) Light-evoked IPSPs (ACSF) are abolished by picrotoxin (PTX). Scale bars, 1 mV, 50 ms. (Inset) Light-evoked APs in a SOM-IN. Scale bars, 20 mV, 50 ms. (**D**) (Left) 2PLSM image of a layer 2/3 pyramidal neuron. Scale bar, 25 μm. (Right) AP-evoked $\Delta Ca^{2+}$ in the spine (Spn) and dendritic shaft (Dnd) indicated by the dashed line. Scale bars, 1 μm, 50 ms. (**E**) (Left) $V_m$ during AP (black), IPSP (blue), and IPSP-AP (red). Scale bars, 2 mV, 100 ms. (Middle and right) $\Delta Ca^{2+}$ (Spn, Dnd) in response to AP (black, blue) or IPSP-AP (red, orange). Scale bars, 1% $\Delta G/G_{sat}$ (where $G$ indicates the amount of green fluorescence), 100 ms. (**F**) $Ca^{2+}$ inhibition for dendritic shafts versus spines. Gray region indicates significant spine inhibition. (**G**) Average $Ca^{2+}$ signals (±SEM) evoked by AP or IPSP-AP for locations showing significant inhibition. Scale bars, 1% $\Delta G/G_{sat}$, 50 ms. (**H**) (Left) $Ca^{2+}$ transients from spine in (E), recorded in PTX. Scale bars, 1% $\Delta G/G_{sat}$, 100 ms. (Right) Average $Ca^{2+}$ inhibition before (ACSF) and after $GABA_A$ block (PTX). *$P < 0.05$ (paired Student's $t$ test).

2PLU of CDNI-glutamate [$2PLU_{Glu}$ (*15*) (methods)] and imaged $\Delta Ca^{2+}$ in spines (Fig. 4, A to D). Inhibition of synaptic $\Delta Ca^{2+}$ was strongly compartmentalized with no correlation between neighboring spines (0.60 ± 0.05 versus 0.98 ± 0.05 for reference spine and adjacent neighbor, respectively, $P < 0.01$; $n = 12$; Pearson $r^2 = 0.18$; $P = 0.17$; Fig. 4, A to D). The $2PLU_{Glu}$-evoked EPSPs were similarly inhibited (Fig. 4, B and D), exhibiting reductions in both amplitude and duration (Fig. 4, D and E) that suggested inhibition might influence synaptic integration. GABAergic input significantly reduced the summation of responses evoked by glutamate uncaging on neighboring spines ($P < 0.05$, $n = 11$, Fig. 4, F to H). The effect on summation was eliminated after blocking *N*-methyl-D-aspartate–type glutamate receptors (NMDARs, $n = 7$, Fig. 4, G and H). Furthermore, summation was not reduced for cases where local $GABA_AR$ activation evoked an IPSP but did not inhibit spine $\Delta Ca^{2+}$ ($n = 8$, fig. S10).

Our results indicate that dendritic spines compartmentalize GABAergic inhibition, limiting both AP- and synaptically evoked $Ca^{2+}$ influx and

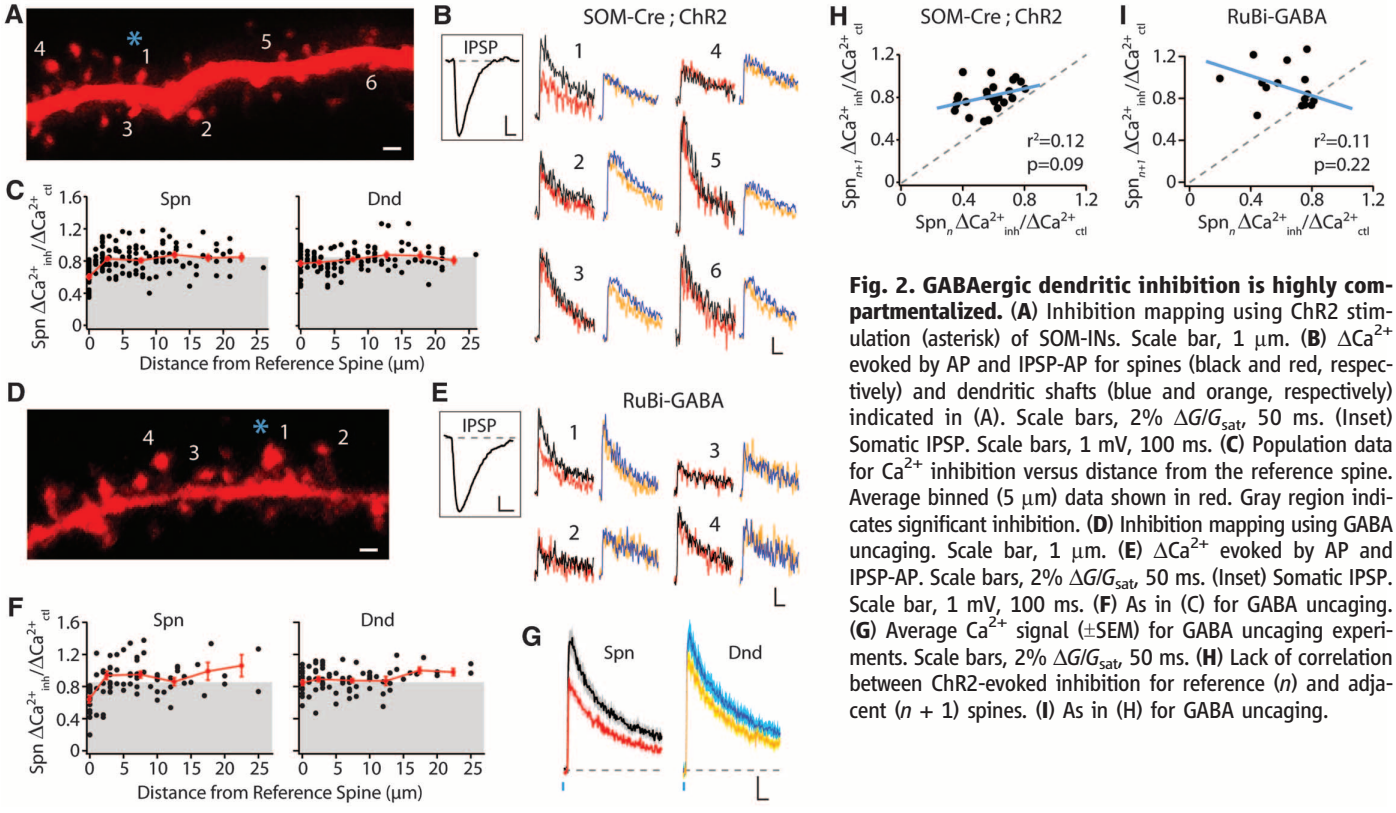


**Fig. 2. GABAergic dendritic inhibition is highly compartmentalized.** (**A**) Inhibition mapping using ChR2 stimulation (asterisk) of SOM-INs. Scale bar, 1 μm. (**B**) $\Delta Ca^{2+}$ evoked by AP and IPSP-AP for spines (black and red, respectively) and dendritic shafts (blue and orange, respectively) indicated in (A). Scale bars, 2% $\Delta G/G_{sat}$, 50 ms. (Inset) Somatic IPSP. Scale bars, 1 mV, 100 ms. (**C**) Population data for $Ca^{2+}$ inhibition versus distance from the reference spine. Average binned (5 μm) data shown in red. Gray region indicates significant inhibition. (**D**) Inhibition mapping using GABA uncaging. Scale bar, 1 μm. (**E**) $\Delta Ca^{2+}$ evoked by AP and IPSP-AP. Scale bars, 2% $\Delta G/G_{sat}$, 50 ms. (Inset) Somatic IPSP. Scale bar, 1 mV, 100 ms. (**F**) As in (C) for GABA uncaging. (**G**) Average $Ca^{2+}$ signal (±SEM) for GABA uncaging experiments. Scale bars, 2% $\Delta G/G_{sat}$, 50 ms. (**H**) Lack of correlation between ChR2-evoked inhibition for reference (*n*) and adjacent (*n* + 1) spines. (**I**) As in (H) for GABA uncaging.

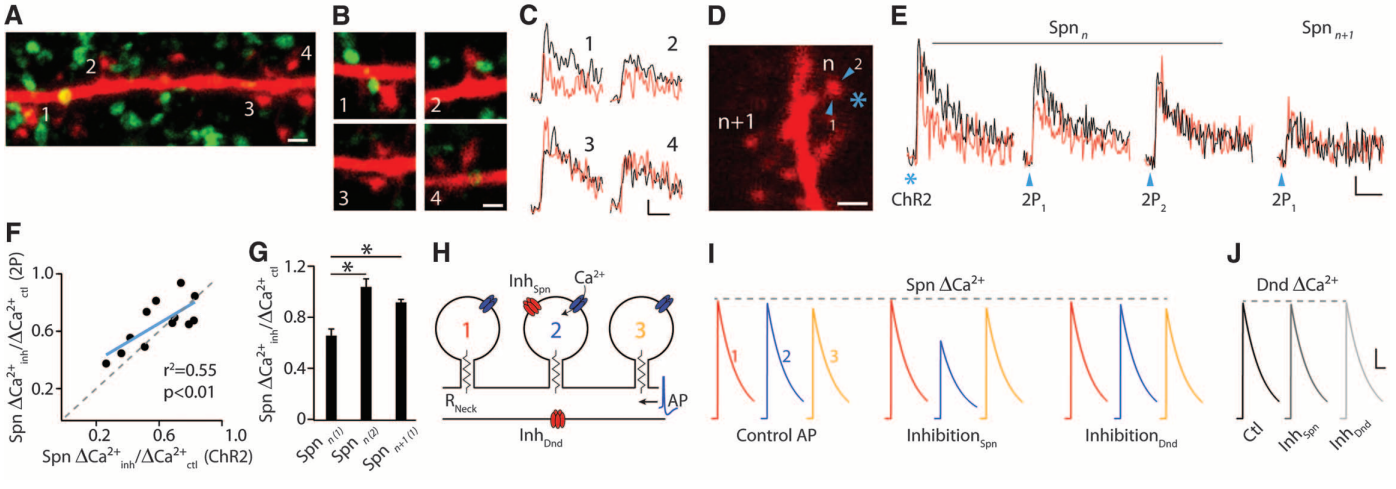


**Fig. 3. GABAergic synapses on spines mediate local $Ca^{2+}$ inhibition.** (**A**) Confocal projection of a dendrite (red) and ChR2–enhanced yellow fluorescent protein–positive boutons (green). Scale bar, 1 μm. (**B**) Single-section images of spines from (A). Scale bar, 1 μm. (**C**) $\Delta Ca^{2+}$ measured in spines from (B) for AP (black) and IPSP-AP (red). Scale bars, 1% $\Delta G/G_{sat}$, 50 ms. (**D**) Inhibition mapping using ChR2 (asterisk) or $2PLU_{GABA}$ (arrowheads). Scale bar, 1 μm. (**E**) $\Delta Ca^{2+}$ in reference spine (*n*) and neighbor (*n* + 1) for AP (black) and IPSP-AP (red). Scale bars, 2% $\Delta G/G_{sat}$, 50 ms. (**F**) Correlation between ChR2- and $2PLU_{GABA}$-evoked inhibition. (**G**) Average $Ca^{2+}$ inhibition (±SEM) evoked by $2PLU_{GABA}$. (**H**) Computational model of dendritic inhibition. (**I**) Simulated GABAergic input selectively inhibits $\Delta Ca^{2+}$ in spine 2. GABAergic input onto dendritic shaft has minimal effect on $\Delta Ca^{2+}$. (**J**) GABAergic input does not inhibit $Ca^{2+}$ in the dendritic shaft. Scale bars in (I) and (J), 100 nM, 100 ms. *$P < 0.05$ (paired Student's *t* test).

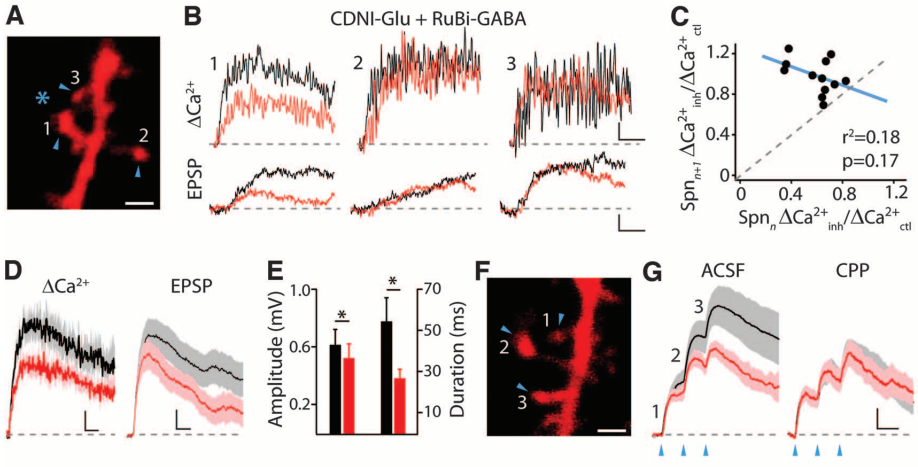


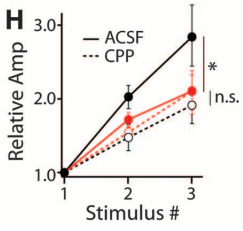


**Fig. 4. Dendritic inhibition regulates synaptic integration.** (**A**) Inhibition of responses evoked by $2PLU_{Glu}$ (arrowheads) using one-photon GABA uncaging (asterisk). Scale bar, 1 μm. (**B**) $\Delta Ca^{2+}$ and voltage transients for EPSP (black) and IPSP-EPSP (red) for spines indicated in (**A**). IPSP alone has been subtracted from paired response. Scale bars, 4% $\Delta G/G_{sat}$, 50 ms (top) or 0.1 mV, 5 ms (bottom). (**C**) $Ca^{2+}$ inhibition is not correlated between neighboring spines. (**D**) Average $\Delta Ca^{2+}$ and somatic voltage transients (±SEM) for EPSP alone (black) and IPSP-EPSP (red) pairing. Scale bars, 2% $\Delta G/G_{sat}$, 50 ms (left) or 0.1 mV, 10 ms (right). (**E**) Average amplitude and duration (±SEM) of voltage transients for EPSP (black) and IPSP-EPSP pairing (red). (**F**) Integration of responses evoked by $2PLU_{Glu}$ (arrowheads). Scale bar, 1 μm. (**G**) Average voltage transients (±SEM) for EPSP (black) and IPSP-EPSP (red) evoked by $2PLU_{Glu}$ on three neighboring spines, recorded in control ACSF (left) or with NMDARs blocked by carboxypiperazin-4-yl-propyl-1-phosphonic acid (CPP) (right). Scale bars, 0.25 mV, 20 ms. (**H**) Relative summation of EPSPs (black) or IPSP-EPSPs (red), recorded in control ACSF or with CPP. *$P$ < 0.05 (Wilcoxon matched pairs test); n.s., not significant.

regulating NMDAR-dependent synaptic integration. These findings establish a previously unknown mechanism for the synapse-specific control of $Ca^{2+}$ signaling and downstream cellular processes such as synaptic plasticity.

Theoretical studies suggested that inhibition might regulate dendritic signaling near synaptic contacts [(*16*–*18*), but see (*19*)]. Subsequent experimental data demonstrated that GABA receptors can inhibit regenerative voltage-dependent dendritic spikes, controlling the production of AP bursts at the soma (*6*–*8*, *20*). These findings were mediated in part by $GABA_B$-dependent modulation of VGCCs and NMDARs (*8*, *21*) and suggested that inhibition acts with lower spatial resolution than glutamatergic excitation, which exhibits compartmentalization of electrical and biochemical signals within single spines (*22*, *23*). However, our data indicate that the spine head similarly restricts $GABA_A$-mediated inhibition. The model further suggests that, in addition to the chloride reversal potential, spine neck resistance influences the efficacy of GABAergic synapses onto spine heads as occurs for glutamatergic inputs (*24*–*26*). Notably, our experimental data was closely modeled by using a neck resistance of 520 Mohm, similar to the value reported for hippocampal pyramidal neurons (*26*). Both neck resistance and chloride reversal are modulated by development and experience (*27*, *28*), suggesting the impact of dendritic inhibition may be similarly regulated.

Dendritic $Ca^{2+}$ influx plays a key role in the induction of plasticity at glutamatergic synapses (*29*), and inhibition can serve as a negative regulator of plasticity (*30*–*32*). Our results suggest that this control occurs at a previously unappreciated spatial scale, enabling dendrite-targeting interneurons to influence individual glutamatergic inputs. This observation is particularly relevant given the growing attention to links between perturbed GABAergic inhibition, alterations in developing neuronal circuits, and neuropsychiatric disorders such as schizophrenia and autism (*33*, *34*).

Why do certain spines receive GABAergic inputs? One possibility is that GABA receptors are recruited by the presence of specific glutamatergic afferents, as proposed for thalamorecipient spines in frontal or visual cortex (*35*, *36*). Additionally, recruitment of $GABA_A$ receptors might be activity-dependent (*37*). This hypothesis is supported by evidence that spine-targeting GABAergic inputs exhibit distinctly high rates of turnover in vivo (*12*, *36*). Future experiments are necessary to determine the existence of feedback loops between dendritic $Ca^{2+}$ signals and the formation and stabilization of GABAergic synapses.

### References and Notes


1. A. Gupta, Y. Wang, H. Markram, *Science* **287**, 273 (2000).
2. G. Fishell, B. Rudy, *Annu. Rev. Neurosci.* **34**, 535 (2011).
3. D. Dumitriu, R. Cossart, J. Huang, R. Yuste, *Cereb. Cortex* **17**, 81 (2007).
4. P. Somogyi, G. Tamás, R. Lujan, E. H. Buhl, *Brain Res. Brain Res. Rev.* **26**, 113 (1998).
5. Y. Wang *et al.*, *J. Physiol.* **561**, 65 (2004).
6. R. Miles, K. Tóth, A. I. Gulyás, N. Hájos, T. F. Freund, *Neuron* **16**, 815 (1996).
7. H. Tsubokawa, W. N. Ross, *J. Neurophysiol.* **76**, 2896 (1996).
8. E. Pérez-Garci, M. Gassmann, B. Bettler, M. E. Larkum, *Neuron* **50**, 603 (2006).
9. H. Taniguchi *et al.*, *Neuron* **71**, 995 (2011).
10. F. Zhang, L. P. Wang, E. S. Boyden, K. Deisseroth, *Nat. Methods* **3**, 785 (2006).
11. E. M. Rial Verde, L. Zayat, R. Etchenique, R. Yuste, *Front. Neural Circuits* **2**, 2 (2008).
12. J. L. Chen *et al.*, *Neuron* **74**, 361 (2012).
13. G. Tamás, E. H. Buhl, P. Somogyi, *J. Physiol.* **500**, 715 (1997).
14. G. C. Ellis-Davies, M. Matsuzaki, M. Paukert, H. Kasai, D. E. Bergles, *J. Neurosci.* **27**, 6601 (2007).
15. M. Matsuzaki, T. Hayama, H. Kasai, G. C. Ellis-Davies, *Nat. Chem. Biol.* **6**, 255 (2010).
16. C. Koch, T. Poggio, *Proc. R. Soc. Lond. B Biol. Sci.* **218**, 455 (1983).
17. C. Koch, T. Poggio, V. Torre, *Proc. Natl. Acad. Sci. U.S.A.* **80**, 2799 (1983).
18. I. Segev, W. Rall, *J. Neurophysiol.* **60**, 499 (1988).
19. N. Qian, T. J. Sejnowski, *Proc. Natl. Acad. Sci. U.S.A.* **87**, 8145 (1990).
20. M. Jadi, A. Polsky, J. Schiller, B. W. Mel, *PLOS Comput. Biol.* **8**, e1002550 (2012).
21. J. R. Chalifoux, A. G. Carter, *Neuron* **66**, 101 (2010).
22. V. A. Alvarez, B. L. Sabatini, *Annu. Rev. Neurosci.* **30**, 79 (2007).
23. M. Matsuzaki, N. Honkura, G. C. Ellis-Davies, H. Kasai, *Nature* **429**, 761 (2004).
24. B. L. Bloodgood, A. J. Giessel, B. L. Sabatini, *PLoS Biol.* **7**, e1000190 (2009).
25. A. Grunditz, N. Holbro, L. Tian, Y. Zuo, T. G. Oertner, *J. Neurosci.* **28**, 13457 (2008).
26. M. T. Harnett, J. K. Makara, N. Spruston, W. L. Kath, J. C. Magee, *Nature* **491**, 599 (2012).
27. B. L. Bloodgood, B. L. Sabatini, *Science* **310**, 866 (2005).
28. H. Fiumelli, M. A. Woodin, *Curr. Opin. Neurobiol.* **17**, 81 (2007).
29. P. J. Sjöström, S. B. Nelson, *Curr. Opin. Neurobiol.* **12**, 305 (2002).
30. J. J. Couey *et al.*, *Neuron* **54**, 73 (2007).
31. H. Lu, P. L. Cheng, B. K. Lim, N. Khoshnevisrad, M. M. Poo, *Neuron* **67**, 821 (2010).
32. H. Wigström, B. Gustafsson, *Nature* **301**, 603 (1983).
33. G. Gonzalez-Burgos, T. Hashimoto, D. A. Lewis, *Curr. Psychiatry Rep.* **12**, 335 (2010).
34. J. L. Rubenstein, M. M. Merzenich, *Genes Brain Behav.* **2**, 255 (2003).
35. Y. Kubota, S. Hatada, S. Kondo, F. Karube, Y. Kawaguchi, *J. Neurosci.* **27**, 1139 (2007).
36. D. van Versendaal *et al.*, *Neuron* **74**, 374 (2012).
37. E. Baho, G. Di Cristo, *J. Neurosci.* **32**, 911 (2012).



**Acknowledgments:** The authors thank G. M. Shepherd for discussions of spine function and P. DeCamilli, S. Tomita, J. Cardin, and members of the Higley laboratory for comments during the preparation of this manuscript. ChR2 plasmids were a gift from K. Deisseroth, Stanford University; TTA-A2 was a gift from B. Bean, Harvard Medical School; SOM-Cre mice were provided by J. Huang, Cold Spring Harbor Laboratory. The work was funded by grants from the Epilepsy Foundation (C.Q.C. and M.J.H.), the Yale Brown-Coxe Memorial Fund (G.L.), the Klingenstein Foundation (M.J.H.), the Sloan Foundation (M.J.H.), the Human Frontier Science Project (G.C.R.E.-D.), and awards from the NIH: NS011613 (N.T.C.), DC009977 (N.T.C. and T.M.M.), MH099045 (M.J.H.), and GM053395 and NS069720 (G.C.R.E.-D.).


### Supplementary Materials

www.sciencemag.org/cgi/content/full/340/6133/759/DC1
Materials and Methods
Figs. S1 to S10
References (*38*–*42*)


19 December 2012; accepted 6 March 2013
10.1126/science.1234274